NRC Research Press

ARTICLE

Mapping attributes of Canada's forests at moderate resolution through *k*NN and MODIS imagery

A. Beaudoin, P.Y. Bernier, L. Guindon, P. Villemaire, X.J. Guo, G. Stinson, T. Bergeron, S. Magnussen, and R.J. Hall

Abstract: Canada's National Forest Inventory (NFI) sampling program is designed to support reporting on forests at the national scale. On the other hand, continuous maps of forest attributes are required to support strategic analyses of regional policy and management issues. We have therefore produced maps covering 4.03×10^6 km^2 of inventoried forest area for the 2001 base year using standardised observations from the NFI photo plots (PP) as reference data. We used the *k* nearest neighbours (*k*NN) method with 26 geospatial data layers including MODIS spectral data and climatic and topographic variables to produce maps of 127 forest attributes at a 250 × 250 m resolution. The stand-level attributes include land cover, structure, and tree species relative abundance. In this article, we report only on total live aboveground tree biomass, with all other attributes covered in the supplementary data (http://nrcresearchpress.com/doi/suppl/10.1139/cjfr-2013-0401). In general, deviations in predicted pixel-level values from those in a PP validation set are greater in mountainous regions and in areas with either low biomass or sparse PP sampling. Predicted pixel-level values are overestimated at small observed values and underestimated at large ones. Accuracy measures are improved through the spatial aggregation of pixels to 1 km^2 and beyond. Overall, these new products provide unique baseline information for strategic-level analyses of forests (https://nfi.nfis.org).

Key words: nonparametric method, remote sensing, boreal forest, stand attribute, biomass, composition, national baseline inventory.

Résumé : L'Inventaire forestier national (IFN) du Canada est un programme d'échantillonnage conçu pour appuyer la production de rapports sur les forêts à l'échelle nationale. D'autre part, les cartes continues d'attributs forestiers sont nécessaires pour appuyer les analyses stratégiques des problématiques régionales de politique et d'aménagement. Nous avons donc produit des cartes couvrant $4{,}03 \times 10^6$ km^2 de surface forestière inventoriée en 2001 à partir d'observations normalisées provenant des placettes photos de l'IFN utilisées comme données de référence. Nous avons utilisé la méthode des *k* plus proches voisins (*k*NN) avec 26 couches de données géospatiales, y compris les données spectrales MODIS et les variables climatiques et topographiques, pour produire les cartes de 127 attributs forestiers à une résolution de 250 × 250 m. Les attributs à l'échelle du peuplement comprennent le type de couverture terrestre, la structure et l'abondance relative des espèces d'arbres. Dans cet article, nous rapportons seulement la biomasse totale aérienne et vivante des arbres. Tous les autres attributs abordés sont présentés dans la section matériel supplémentaire (http://nrcresearchpress.com/doi/suppl/10.1139/cjfr-2013-0401). En général, les écarts des valeurs prédites à l'échelle du pixel par rapport à celles des placettes photos de validation, sont plus importants dans les régions montagneuses et dans les zones où, soit la biomasse, soit le taux d'échantillonnage de placettes photos est faible. Les valeurs prédites à l'échelle du pixel sont surestimées lorsque les valeurs observées sont petites et sous-estimées lorsqu'elles sont grandes. Les mesures de précision sont améliorées grâce à l'agrégation spatiale des pixels sur 1 km^2 et plus. Dans l'ensemble, ces nouveaux produits fournissent des informations de base uniques pour les analyses stratégiques des forêts (https://nfi.nfis.org). [Traduit par la Rédaction]

Mots-clés : méthode non paramétrique, télédétection, forêt boréale, attribut de peuplement, biomasse, composition, inventaire national de référence.

Introduction

Canada's forests and wooded lands cover 40% of its territory and constitute one-tenth of the world's forest area (National Forest Inventory 2010). Provincial and territorial governments are responsible for forested lands within their boundaries and deploy forest inventory programs with standards, intensities, and frequencies designed to fit their specific forest management needs. Differences in inventory data sets among such programs make their integration at the national level difficult. Canada's National Forest Inventory (NFI), a collaborative effort between the federal government and the provincial and territorial forest management agencies, was therefore developed to bridge that gap (Gillis et al. 2005). One of the main NFI products is a set of photo plots (PP), 2 × 2 km square sampling units centred on the intersections of a grid of a nominal 20 × 20 km format that covers all of Canada. The PP sampling thus covers 1% of the forests of Canada. Its systematic sampling provides estimates of selected forest properties across all forested landscapes in support of forest assessment and report-

Received 25 September 2013. Accepted 24 January 2014.

A. Beaudoin, P.Y. Bernier, L. Guindon, P. Villemaire, X.J. Guo, and T. Bergeron.* Natural Resources Canada, Canadian Forest Service, Laurentian Forestry Centre, P.O. Box 10380 Stn. Sainte-Foy, Québec, QC G1V 4C7, Canada.
G. Stinson and S. Magnussen. Natural Resources Canada, Canadian Forest Service, Pacific Forestry Centre, 506 West Burnside Road, Victoria, BC V8Z 1M5, Canada.
R.J. Hall. Natural Resources Canada, Canadian Forest Service, Northern Forestry Centre, 5320-122nd Street, Edmonton, AB T6H 3S5, Canada.
Corresponding author: A. Beaudoin (e-mail: andre.beaudoin@nrcan.gc.ca).
*Present address: AECOM-Quebec, 4700, boul. Wilfrid-Hamel, Quebec, QC G1P 2J9, Canada.

Fig. 1. Map of Canada's 15 ecozones (black lines) covering six well-inventoried forested ecozones (open areas), six partly or noninventoried forested ecozones (light grey), and three nonforested Arctic ecozones (dark grey). The Pacific Maritime, Montane Cordillera, and Boreal Cordillera ecozones are characterized by high relief. Also shown are provincial and territorial boundaries (grey lines) and the location of the NFI photo plots from which we extracted reference and validation pixels for *k*NN prediction. (Base map source: Natural Resources Canada under the Open Government Licence – Canada (http://data.gc.ca/eng/open-government-licence-canada.)

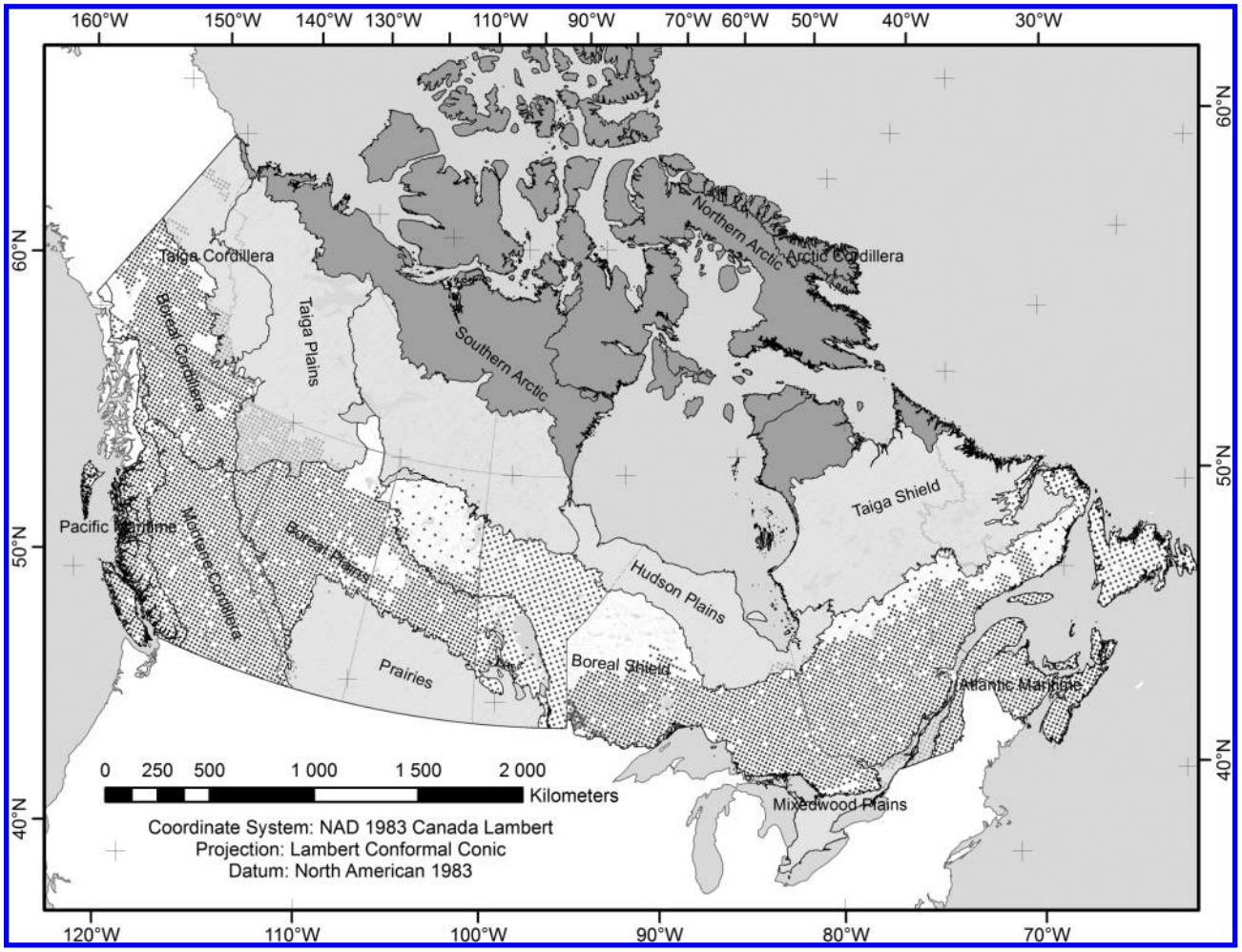

ing at the scale of terrestrial ecozones (Ecological Stratification Working Group 1996).

In addition to national or ecozone-level reporting, many applications such as evaluations of timber losses from forest fires or the spread of invasive insects based on host tree species abundance require a spatially explicit coverage of forest attributes with units and definitions harmonized across jurisdictional boundaries. A decision was therefore made to develop forest attribute map products using the attribute values from the PPs as the source of reference information and remote sensing data sets as the main source of predictor variables. The design criteria for the output product were that (*i*) the spatial resolution and accuracy would be sufficient to support strategic-level reporting at regional to national scales and (*ii*) the resulting spatial data sets would be updatable between NFI re-measurements of PPs. We therefore selected the 250 × 250 m pixel (250 m hereafter) of the satellite-borne moderate resolution imaging spectroradiometer (MODIS) as the resolution of the output map product.

Following a preliminary trial on a pilot region (Beaudoin et al. 2011), we also chose to use the nonparametric *k* nearest neighbours (*k*NN) method as our basic mapping method because it met three basic criteria: (*i*) the capacity to predict simultaneously a large set of attributes while preserving their among-attribute functional relationships, (*ii*) a relative simplicity and cost effectiveness to implement across a large country such as Canada, and, importantly, (*iii*) a successful track record of application within national forest inventory programs. This choice is also supported by Brosofske et al. (2014) for application to forest inventory mapping.

The *k*NN method is a multivariate nonparametric prediction procedure that uses a set of predictor feature variables (*X*) to match each target pixel to a number (*k*) of most similar (nearest neighbours or NN) reference pixels for which values of response variables (*Y*) are known (McRoberts 2012). Feature variables are predictor variables for which values are known for both target and reference units and are used to match one to the other. The similarity measure between a target pixel and reference pixels can be given by any of several distance metrics such as the Euclidian distance (McRoberts 2009). First proposed for application in forestry using satellite data by Tomppo (1991), this method and its many variants have now been tested or applied successfully within forest inventory programs in many countries (Tomppo 2006; McRoberts 2012; Wilson et al, 2013). As a consequence, there is now a relatively large body of knowledge related to *k*NN application to forestry that can be drawn upon for our specific needs.

The objectives of this work were therefore (1) to produce forest attribute maps for the baseline year 2001 using an optimized *k*NN procedure for a broad suite of PP attributes across the well-inventoried forests of Canada and (2) to quantify the accuracy of

Table 1. Canada's 12 forested ecozones as in Fig. 1 along with National Forest Inventory (NFI) photo-plot (PP) inventory status: (A) count for all and fully inventoried 2 × 2 km² NFI PP, (B) count of 250 m reference (Ref) and validation (Val) pixel samples, and (C) descriptive statistics for aboveground biomass (AGB) for the reference sample set.

			(A) 2 × 2 km² NFI PP count		(B) Count of 250 m ref–val pixel samples		(C) AGB (t/ha) descriptive statistics (reference samples)			
Forested ecozones	Inventory†	Area,‡ 10^6 km²	All	Inventoried§	Ref	Val	Minimum	Maximum	Mean	SD
Boreal Shield	$X_{g,i}$	1.92	4835	2961	7695	3321	0.0	246.4	58.6	42.2
Taiga Shield	0	1.39	3594	15	32	17	0.0	128.9	39.9	36.3
Boreal Plains	$X_{g,i}$	0.74	1879	1463	3828	1573	0.0	287.6	46.1	44.8
Taiga Plains	x	0.66	1692	240	644	272	1.3	213.8	54.8	52.1
Montane Cordillera*	X	0.49	1252	1204	2971	1358	0.0	420.6	104.8	91.5
Boreal Cordillera*	X_g	0.47	1208	1030	2687	1185	0.0	225.0	31.9	43.8
Prairies	0	0.47	1182	23	50	24	4.4	111.5	18.2	22.6
Hudson Plains	0	0.37	936	18	41	20	0.8	131.8	36.6	30.1
Taiga Cordillera*	x	0.27	709	104	278	109	0.0	117.3	15.3	23.5
Pacific Maritime*	X	0.21	577	512	1227	505	0.0	724.0	151.3	161.6
Atlantic Maritime	X	0.20	538	519	1290	566	0.0	174.8	64.7	41.1
Mixedwood Plains	x	0.17	318	113	294	105	0.0	175.1	38.6	44.3
Six well-inventoried ecozones		4.03	10289	7689	19698	8508				
All ecozones		7.36	18720	8202	21037	9055				

Note: Ecozones are sorted by decreasing area size, with the shaded ones being poorly inventoried.
*Mountainous ecozones.
†Within the NFI PP establishment database: X, extensive (g, significant spatial gaps; i, variable areal intensity); x, poor (sparse or local); 0, practically nonexistent.
‡Area source: https://nfi.nfis.org/publications/standard_reports/NFI_T1_LC_AREA_en.html.
§With full suite of attributes.

the predicted attribute values relative to a reserved PP validation set of attribute values at spatial scales from pixels to ecozones.

Materials and methods

Mapping area, NFI PPs, and response variables

The potential mapping area for the present exercise covers the 12 forested ecozones of Canada for a total area of about 7.4 × 10^6 km² (Fig. 1; Table 1). The NFI PP data, which were established, collected, and compiled over a 7-year period between 2000 and 2006, form a large sampling set across these ecozones in which definitions and units of forest attributes are harmonized across all jurisdictions. The PP sampling intensity and the completeness and quality of NFI information within PPs are far greater within the managed forests because of existing forest inventory programs and much lower in the unmanaged forests located mostly in northern Canada. The current mapping effort is therefore based on the 8202 PPs with complete forest attribute information of the 18 720 PPs across Canada (Fig. 1; Table 1). Although predictions were made for all 12 forested ecozones, the mapping effort is nominally limited to the 4.03 × 10^6 km² of six well-inventoried ecozones within which accuracy measures can be generated. Predicted values in other ecozones should be used with caution.

Each 2 km × 2 km PP is composed of forest polygons (stands) delineated from photo interpretation. Each stand has been assigned values for land use, land cover, and forest structure attributes from which 127 forest attributes were selected as a set of response variables (*Y*) to be predicted across target pixels (Supplementary Table S1).[1] This set includes (1) four land cover attributes derived from photo interpretation related to vegetated and treed proportions, (2) 11 stand structures (age, height, and crown closure derived from photo interpretation, as well as merchantable volume provided by provinces used by NFI staff to estimate total volume and aboveground biomass based on Boudewyn et al. (2007) models), and (3) 112 forest species composition as percent abundance. For the sake of simplicity, in this paper, we report on only one of these attributes, total live aboveground tree biomass (AGB, tonnes (t) per hectare). The accuracy measures of the resulting *k*NN predictions are available for all attributes in Supplementary Table S2.

The stands within the selected PPs along with their suite of 127 attributes were first rasterized to a 25 × 25 m grid using NN interpolation. The resulting 127 raster layers were then aggregated to the 250 m MODIS grid through spatial averaging. Averaging was done with biomass weighting for some of the structural attributes to retain the original functional relationships among the PP attributes (Supplementary Table S1). Only the 250 m pixels fully within a PP boundary were retained as potential *k*NN samples (Fig. 2). Spatial analyses based on semivariograms had shown that spatial autocorrelation became negligible at distances greater than about 1.5 km. We therefore retained only the four corner pixels within each PP for further analyses (Fig. 2). Pixels were also removed if they had been affected by fire or harvesting after 2001, our *k*NN mapping year (for the change detection method, see Guindon et al. 2011).

The remaining corner pixels (N = 30 092) were split into a reference and validation (ref–val) set. Tests carried out within a commonly used range (Picard and Berk 1990) of percent ref–val splits (50%–50%, 70%–30%, and 80%–20%) randomly replicated 30 times each revealed a maximum difference of 1.2% among the mean values of two *k*NN accuracy measures (see description below) across the three splits. As a consequence, we retained the commonly used 70%–30% data split (N_{ref} = 21 037 and N_{val} = 9055) to carry out the analysis (Table 1).

Selecting feature variables

We assembled a set of 31 Canada-wide continuous geospatial layers covering all 12 forested ecozones to be used as predictor *X* feature variables. This set included 18 spectral reflectance vari-

[1]Supplementary data are available with the article through the journal Web site at http://nrcresearchpress.com/doi/suppl/10.1139/cjfr-2013-0401.

Fig. 2. Schematics of the application of the 250 m MODIS pixel grid to a single 2 × 2 km² NFI photo plot (PP) with its photo-interpreted forest polygons along with PP total live aboveground biomass (AGB, t/ha) estimates in grey scale. As shown, only pixels fully contained within the PP are retained, and only corner pixels are used as either reference or validation pixels.

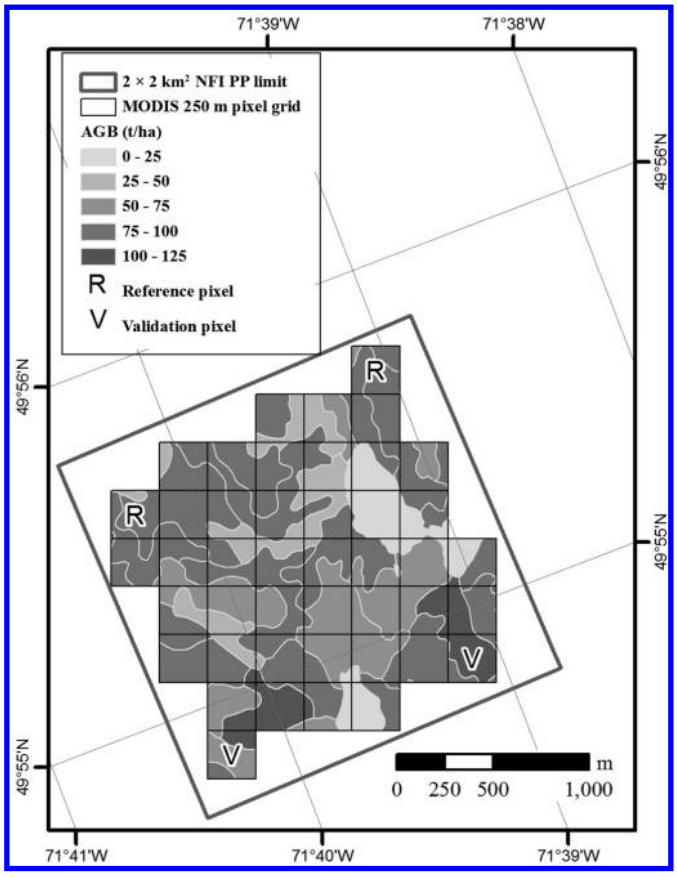

ables, nine climatic variables, three topographic variables, and one permanent land cover class (Table 2) as in similar studies (e.g., Brosofske et al. 2014). All variables were standardized to values between –1 and 1 (*Z* score) to avoid scale effects (LeMay and Temesgen 2005).

Scenes from TERRA MODIS level 1.B geolocated top-of-atmosphere radiance data (MOD02) for 2001 summer (July–August) and winter (January–February) were processed by the Canada Centre for Remote Sensing to produce orthorectified seasonal mosaics of composite surface reflectance at 250 m resolution (Pouliot et al. 2009). Each seasonal mosaic is based on two averaged monthly (5 × 10 day) composites (Luo et al. 2008) with various geometric and radiometric corrections applied, including the downscaling of band 6 from 500 m to 250 m resolution (Trishchenko et al. 2006). The resulting spectral features (Table 2) include the summer and winter reflectance data in bands 1, 2, and 6 at 250 m resolution (see colour composites in Supplementary Fig. S1), as well as six spectral indices derived from summer and winter reflectance data (Pouliot et al. 2009).

Climatic data (30-year normals, 1970–2000) were obtained from 1 × 1 km resolution interpolated meteorological data (McKenney et al. 2011) re-sampled to the 250 m MODIS pixel grid using cubic interpolation to generate appropriate climatic feature variables. These include three variables related to temperature, three related to precipitation, two indices of soil moisture availability, and mean annual incoming shortwave radiation. Slope, cosine of aspect angle, and elevation were derived from a SRTM-based 90 m digital elevation model (DEM) (Farr et al. 2007) re-sampled at the 250 m MODIS grid using cubic interpolation. Finally, the percent water cover by pixel was extracted from a 2000 Canada-wide 25 × 25 m resolution land cover map (Wulder et al. 2008) aggregated to 250 m through spatial averaging.

We explored the possibility of reducing the number of feature variables to avoid detrimental effects on *k*NN prediction accuracy due to the inclusion of *X* variables unrelated to *Y* response variables (McRoberts et al. 2002). We used the hybrid least absolute shrinkage and selection operator (hybrid-LASSO (HL); Efron et al. 2004) method to rank all feature variables according to the strength of their relationship to each *Y* of a subset of 27 of 127 response variables including all four land cover and 11 stand structure attributes along with 12 tree species abundance attributes representing key broad-leaved – needle-leaved and tolerant–intolerant species combinations and close to 60% of total biomass in the PP data set. These rankings based on adjusted R^2 (adj. R^2) values for individual *Y* variables were then merged into a single set, and *X* variables with consistently low ranking were deleted from the set. The adj. R^2 quantifies the strength of the relationship between the feature variable and PP attribute and has a range of 0 to 1. Redundant *X* variables were also removed from the set when their marginal contribution to adj. R^2 was less than 1% to provide a reduced *X* set.

Optimizing *k*NN parameters

As mentioned above, the application of the *k*NN method entails identifying the *k* nearest reference pixels in the feature space for each target pixel. Values of each *Y* within these *k* nearest pixels are then averaged and assigned to the target pixel. Formally, the estimate $\tilde{y}_i$, the resulting mean value of variable *Y* for target pixel *i*, is calculated as in McRoberts (2012):

$$\tilde{y}_i = \left(\sum_{j=1}^{k} w_j^i \right)^{-1} \sum_{j=1}^{k} w_j^i y_j^i \quad (1)$$

where $\{y_j^i; j = 1,\ldots,k\}$ is the set of observations for the *k* reference set pixels nearest in feature space to the *i*th target set pixel, as calculated using a given distance metric (dm). The weights w_j^i used for each of the *k* pixels in the averaging process are calculated as

$$w_j^i = d_{ij}^{-t} \quad (2)$$

where d_{ij} is the distance in feature space between the *i*th target pixel and the *j*th nearest reference pixel calculated using a given dm, and exponent *t* is used to modulate the impact of distance in the weighting (usually $t = 0$, 1, or 2).

Optimized selection of the three *k*NN parameters (dm, *t*, and *k*) was performed through the analysis of *k*NN predictions using the yaImpute R package (Crookston and Finley 2008) and the ref–val set. Predictions using the reduced set of *X* feature variables were done only for the Euclidian (EUC) dm as our privileged approach and were compared against predictions with the complete *X* set (31 feature variables) along with four popular distance metrics (Hudak et al. 2008), i.e., EUC, Mahalanobis (MAH), gradient nearest neighbour (GNN), and most similar neighbour (MSN), using the *k* neighbours version as in Packanen and Maltamo (2007). The Mahalanobis dm handles covariance among *X*s, while the two other variants handle *X*–*Y* correlations and provide ranking and weighting to features, respectively, through canonical correspondence and canonical correlation analyses. For all of these combinations, *t* values were restricted to 0 or 1 and *k* values were between 1 and 15 based on preliminary results from application to a pilot region (Beaudoin et al. 2011).

For each of the five *X*–dm–*t* combinations, we computed the multivariate goodness of fit criterion *T* (McRoberts 2012) across the range of *k* values using the following equation based on the sample reference set:

Table 2. Characteristics of the 31 geospatial layers across Canada initially selected as feature variables (X) for *k* nearest neighbours (*k*NN) prediction.

Category and subcategory	Feature (description)	Label	Units	Initial resolution
Spectral				
Spectral bands	Summer and winter MODIS band 1 (red band, 620–670 nm)	B1s, B1w	—	250 m (B6w and B6s at 500 m)
	Summer and winter MODIS band 2 (near-infrared band, 841–876 nm)	B2s, B1w	—	
	Summer and winter MODIS band 6 (shortwave infrared band, 1628–1652 nm)	B6s, B6w	—	
Spectral indices	Summer and winter NDVI (normalized difference vegetation index)	NDVIs, NDVIw	—	
	Summer and winter SAVI (soil adjusted vegetation index)	SAVIs, SAVIw	—	
	Summer and winter RSR (reduced simple ratio)	RSRs, RSRw	—	
	Summer and winter WDVI (wide dynamic range vegetation index)	WDVIs, WDVIw	—	
	Summer and winter NDMI (normalized difference moisture index)	NDMIs, NDMIw	—	
	Summer and winter GEMI (global environment monitoring index)	GEMIs, GEMIw	—	
Climatic				
Temperature	Mean annual temperature (mean of all of the monthly mean temperatures)	MAT	°C	1000 m
	Mean minimum daily temperature of coldest month (lowest temperature of any monthly minimum temperature)	MMIN	°C	
	Mean maximum daily temperature of hottest month (highest temperature of any monthly maximum temperature)	MMAX	°C	
Precipitation	Total annual precipitation (sum of all the monthly precipitation estimates)	TAP	mm	
	Precipitation of warmest quarter (total precipitation over warmest quarter of the year)	PWQ	mm	
	Precipitation of coldest quarter (total precipitation over the coldest quarter of the year)	PCQ	mm	
Moisture	Annual climate moisture index (ACMI = *P*–PET, where *P* is annual precipitation and PET is annual potential evapotranspiration)	ACMI	cm/year	
	Summer climate moisture index (summer CMI over months of June to September)	SCMI	cm/summer	
Radiation	Mean annual radiation	MAR	MJ/m²	
Topographic	Terrain altitude (altitude of terrain above sea level from SRTM DEM)	ALT	m	90 m
	Terrain slope (local slope calculated on DEM)	SLOPE	°	
	Terrain aspect angle (cosine of terrain aspect)	ASPECT	—	
Land cover, hydrography	Proportion of water bodies (from 2000 EOSD land cover map)	WATER	%	25 m

Note: Shaded feature layers along with labels represent the five variables (four winter ones for spectral variables) not retained for the *k*NN prediction, as per the criteria described in the text.

$$T = \sum_{y=1}^{Y} w_y T_y^2 \quad (3)$$

where *y* represents one of the 27 (*Y*) response variables used in the HL procedure, w_y is a set of weights that sums to 1 (here all set equally to 1/*Y*), and T_y^2 is the fractional amount of variance in response variable *y* explained by the *k*NN prediction. The choice of the best *X*–dm–*t* combination was based on a comparison of *T* values among curves. In addition, graph of root mean square deviation vs. *k* derived from the validation set (eq. 5) was used as a univariate accuracy measure (McRoberts 2012) to further assess the choice of the optimal combination for AGB. For a given X–dm–*t* combination, the value of *k* was deemed optimal when its corresponding value of *T* reached 0.95 of T_{max}, where T_{max} is the maximal value of *T* on the curve. This result was further checked against the one found using RMSD% curve for AGB (value of *k* when RMSD% equalled 1.05 of RMSD%$_{min}$). The optimization exercise was repeated for the 30 random replicates, yielding values of means and standard errors of *T*, RMSD%, and optimal *k* values. These values were then used to compare the EUC *k*NN using the reduced *X* set with other dm–*t* combinations using the complete *X* set.

kNN mapping, diagnostic, and accuracy measures

Following this selection process (see Results), the Euclidian *k*NN with $t = 0$ and $k = 6$ using the reduced *X* set was implemented across Canada for mapping all 127 response variables using a single realization of the ref–val set. No a priori stratification of the country was used to geographically restrain the recruitment of neighbours, but the use of climatic features promoted the recruitment of neighbours from climatically similar areas. Maps of attributes were produced using an in-house C++ *k*NN routine (*k*NNMapping) that provides very fast and exact *k*NN prediction using the approximate nearest neighbor (ANN) library (Mount and Arya 2010).

The *k*NNMapping routine also produces maps of three diagnostic variables for evaluating sampling representativeness and deficiencies. The first of them is a variance estimator $\hat{\sigma}_i$ in the absence of spatial autocorrelation (McRoberts et al. 2007) among the *k* neighbours for each attribute:

$$\hat{\sigma}_i^2 = \frac{\sum_{j=1}^{k} (y_{i,j} - \hat{\mu}_i)^2}{k - 1} \quad (4a)$$

where $y_{i,j}$ is the value of the PP attribute for neighbour *j* to pixel *i* and $\hat{\mu}_i = \tilde{y}_i$ is the predicted mean of the *k* neighbours. This estimator was computed for each pixel *i* and was used to calculate a coefficient of variation (CV, %):

$$CV_i = \frac{\sqrt{\hat{\sigma}_i^2}}{\tilde{y}_i} \times 100 \quad (4b)$$

where $\tilde{y}_i$ is the *k*NN predicted value. The two other diagnostic variables are the Euclidian (D_{euc}) and geographic (D_{geo}) recruitment distances of the *k* neighbours for each target pixel to assess

Fig. 3. (A) Multivariate *T* curves vs. *k* based on 27 response variables and (B) univariate RMSD% curves vs. *k* for AGB for five combinations X–dm–*t*, including two *X* feature sets (complete set, 31X; HL-reduced set, 26X), four *k*NN distance metrics (EUC, MAH, GNN, and MSN), all with no weighting (*t* = 0). Mean values are from 30 replicates; standard errors are very small and are not included for clarity.

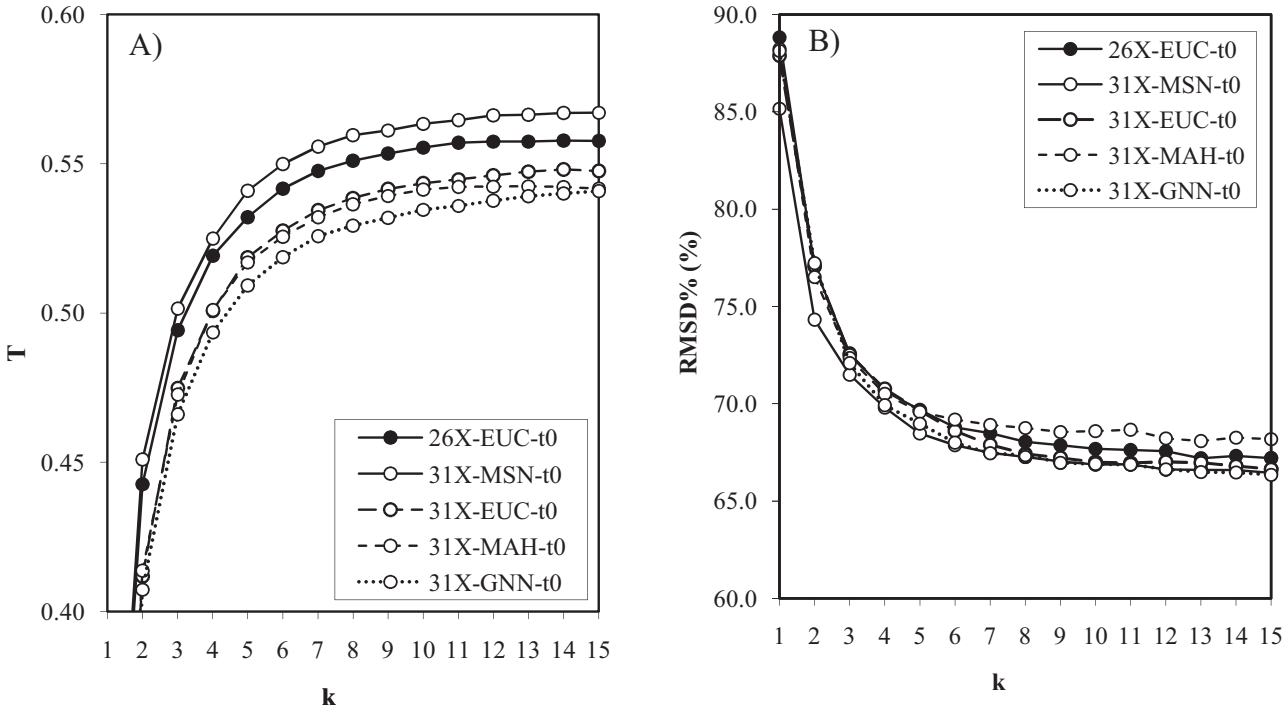

sampling distances in the feature space and in the geographical space, respectively.

Pixel-level accuracy of predicted values relative to "observed" PP attribute values of the 30% validation set was assessed graphically through an observed vs. predicted graph by binned groups of $n = 100$ samples ranked in order of increasing observed value as in McRoberts (2009). Commonly used accuracy measures were also computed: pseudo coefficient of determination R^2 (hereafter R^2, equation not shown), relative root mean-squared deviation (RMSD%) (Crookston and Finley 2008), and relative mean deviation (MD%):

$$\text{RMSD\%}_m = \frac{\sqrt{\frac{1}{n}\sum_{i=1}^{n}(\tilde{y}_i - y_i)^2}}{\bar{y}} \times 100 \quad (5)$$

$$\text{MD\%}_m = \frac{\frac{1}{n}\sum_{i=1}^{n}(\tilde{y}_i - y_i)}{\bar{y}} \times 100 \quad (6)$$

where for a validation set m containing n pixels indexed i, $\tilde{y}_i$ is the *k*NN predicted value, and y_i and $\bar{y}$ are, respectively, the pixel value and mean value of the observed PP attribute. Means and standard errors of these measures were obtained with the 30 replicates to take into account the impact of random sample realizations of the ref–val split (LeMay and Temesgen 2005).

The calculations were also performed for AGB on 3 × 3, 5 × 5, and 7 × 7 pixel windows (750, 1250, and 1750 m, respectively) centred on PP centroids to test the effect of spatial aggregation on prediction accuracy. This last procedure was applicable only to 379 of the 8202 PPs available due to PP boundary effects (Fig. 2).

Finally, ecozone-level estimates of total AGB (tonnes (t)) obtained by *k*NN were compared with PP-based total AGB estimates. For our comparison, AGB values were summed across tiles within each ecozone. A tile is the 20 × 20 km² square centred on a given 2 × 2 km² PP that it represents (1% sample). Tile-level *k*NN AGB is the sum of the within-tile pixel estimates, whereas tile-level PP AGB is the mean AGB value in the original PP data expanded to the tile, with the value of the expansion factor nominally equal to 100.

Results

Feature selection and parameter optimization

Results of the HL procedure show that among all 26 feature variables, spectral feature variables explain the most variance in the land cover and structural attribute categories, whereas climatic feature variables generally explain the most variance in the 10 species abundance attributes due to their relationship to climate. Topographic and land cover (WATER) features have only a modest contribution for all attributes (Supplementary Fig. S2*a*). Depending on the attribute category, best predictor spectral features were B1w and B6s bands and NDVIs and RSRs/w indices, indicative of the usefulness of winter MODIS imagery combined with the summer one. Best climatic features were related to precipitation (PCQ and PWQ) and temperature (MMIN and MAT) (Supplementary Fig. S2*b*). Merging of all HL-selected feature sets relative to each PP attribute and removal of redundant features enabled us to identify and remove four spectral feature variables and one topographic feature variable. We thus retained 26 feature variables of the complete set of 31 (Table 2).

The analysis of mean *T* values resulting from the five *X*–dm–*t* combinations (Fig. 3A) shows that the best fit is obtained with the complete set using the MSN dm (31X-MSN-t0) followed closely by the combination of the reduced set and the Euclidian dm (26X-EUC-t0). Other combinations using the MAH dm and GNN dm have smaller values of *T*. Analyses based on the 30 random replicates show the 31X-MSN-t0 variant to be only slightly better than the simpler 26X-EUC-t0 variant, with differences of –2.1% in mean *T* values and of +1.75% in mean RMSD% values (Fig. 3B) between the

two variants (average across all k values). Finally, each combination above was tested for $t = 1$ relative to $t = 0$, and in all cases, differences were found to be negligible for both T and RMSD% (results not reported). Given its interpretive advantages, we therefore selected the 26X-EUC-t0 variant for the rest of the study. We also selected $k = 6$ based on the optimal values of 5.5 ± 0.1 and 4.4 ± 0.1 obtained from T and RMSD% curves, respectively (Figs. 3A and 3B).

NFI attribute prediction and diagnostics

Maps of predicted AGB (Fig. 4A) along with three diagnostic variables (Figs. 4B, 4C, and 4D) are reported with their ecozone-level mean values (Fig. 5*a*). For the six well-inventoried ecozones, values of CV% are large in the mountainous ecozones of western Canada and in areas of low biomass such as recently disturbed or unproductive forests and agriculture areas (Figs. 4B and 5A), suggesting a greater uncertainty in their predicted AGB values. To the contrary, values of CV% are small across the Boreal Shield ecozone with its moderately flat topography and moderate AGB levels. Values of D_{euc} of the k neighbours from target pixels show a trend similar to that of CV%, further revealing sampling issues in the X feature space for mountainous or low biomass areas (Figs. 4C and 5A). Finally, values of D_{geo} predictably increase in areas where the PP sampling is locally sparse or missing (Figs. 1, 4D, and 5A). Across the six well-inventoried ecozones, mean D_{geo} is of 161 km.

Accuracy assessment at various scales

At the pixel level, binned AGB *k*NN predictions show an overestimation (positive MD%) of smaller values and an underestimation (negative MD%) of larger ones (Fig. 6). The pattern and magnitude of the deviation varies among ecozones and attributes (analysis not shown). When calculated using the complete validation data set across its 30 replicates, mean pixel-level values of MD%, RMSD%, and R^2 for AGB are 1.47% ± 0.14%, 69.22% ± 0.18%, and 0.62 ± 0.002, respectively. These mean accuracy measures vary substantially across the six managed ecozones and are the best for the large Boreal Shield ecozone (Fig. 5B). Accuracy measures for all attributes (Supplementary Table S2) show that values of $R^2 > 0.30$, RMSD% < 100%, or absolute MD% < 10% were achieved for land cover and structure attributes, as well as for the abundance of the more common tree species.

Pixel aggregation substantially improves all accuracy measures for AGB. Values of R^2 increase by 25% and MD% and RMSD% decrease by about 40% when pixels are spatially aggregated beyond a 1 km² window (Fig. 7). At the level of the six well-inventoried ecozones for totals in AGB, the relative difference between predicted *k*NN-derived AGB and the "measured" expanded PP AGB totals is within ±4% for all but the two mountainous Boreal Cordillera and Montane Cordillera ecozones and is best for the Boreal Shield ecozone. Overall, relative difference for the six well-inventoried ecozones is –1.83% (Table 3).

Discussion

The PP data set was successfully used with MODIS spectral information and other auxiliary feature variables within an optimized Euclidean-based *k*NN prediction method to produce maps of forest attributes across provincial and territorial boundaries for managed forests of Canada. Previously in Canada, various projects have produced land cover maps using either LANDSAT (Wulder et al. 2008) or MODIS imagery (Latifovic et al. 2012), as well as maps of selected forest attributes such as volume and biomass (Hall et al. 2010). However, the present effort is the first to produce a coherent set of quantitative values for such a large suite of forest attributes across Canada's well-inventoried forests.

As mentioned earlier, Finland has been producing *k*NN-based national maps of forest properties but has been using LANDSAT multispectral data (Tomppo et al. 2008) because of its relatively small forest domain and dense field plot system as compared with Canada. We successfully used MODIS data as a cost-effective alternative to LANDSAT to cover much larger areas at the expense of decreased resolution, similarly to the *k*NN-based mapping carried on in the US (Wilson et al. 2012, 2013). Although these studies share their basic NN method with ours, the details of the analyses and resulting accuracies are strongly conditioned by their respective national circumstances.

Accuracy was assessed and analyzed at various scales using a reserved validation set of NFI PP. At the pixel level, the pattern of overestimation of small values and underestimation of large ones (Fig. 6) is typical of *k*NN (Magnussen et al. 2010) and explains the relatively large and variable values of RMSD% (Fig. 5B; Supplementary Table S2). Sources of errors at the pixel level are diverse but certainly include the use of stand-level photo-interpreted or modeled values of forest attributes as "ground truth" in PPs (Magnussen and Russo 2012) compared with actual field plot data such as used in Wilson et al. (2013). Compounding this problem is the use of older aerial photos for extracting values of forest attributes and their resulting temporal mismatch with the 2001 MODIS mosaics. Ongoing updating of PP information by provincial partners should lead to improved *k*NN predictions.

Various geometric and radiometric issues related to the MODIS-based spectral feature variables also contribute to the overall uncertainty. Winter reflectance data, an important predictor of forest cover attributes, are sensitive to the variability in snow cover depth and persistence. Larger CV% values at the prairie–forest ecotone in western Canada (Fig. 4*b*) were found to result from discontinuous snow cover in this low-precipitation area (red patches in Supplementary Fig. S1). Overall, spectral features are prone to radiometric imbalance and residual haze effects within the MODIS mosaic (Pouliot et al. 2009), to decreased geolocation accuracy and increased radiometric distortions in high relief areas (Brosofske et al. 2014), and to spectral saturation (Lu et al. 2012) in areas of large values of forest attributes, particularly in the Pacific Maritime ecozone. Inclusion of additional remotely sensed features such as PALSAR L-band radar backscatter mosaics (Shimada and Ohtaki 2010) could help to reduce the overall uncertainty, particularly for the underestimation of larger biomass values as the L-band signal saturates at a larger biomass level than optical data (Dobson et al. 1992).

The level of uncertainty in the attribute predictions at the pixel level compares favourably with the stand-level uncertainty found by Bernier et al. (2010) for a large operational inventory program in eastern Canada. The highest accuracy was achieved for the Boreal Shield ecozone (Fig. 5B), which represents about 53% of the forest in the six well-inventoried ecozones (Table 1) and 38% of the forest in Canada. The substantial and asymptotic drop in MD% and RMSD% when aggregating pixels beyond a 1 km² window (Fig. 7) supports the use of the *k*NN-predicted spatial data sets for small-area estimation (Katila 2006; McRoberts 2012) for which poor inference statistics are expected using the 1% NFI PP samples. The mass balance of AGB totals is generally well preserved at the ecozone level at the cost of decreased resolution, therefore supporting its use for regional reporting (Table 3).

For species abundance, accuracy measurements for the needle-leaved species group are relatively good but accuracy measures for individual species decrease with decreasing species abundance (Supplementary Fig. S3 and Supplementary Table S2). In spite of all their shortcomings, the *k*NN species-level products provide an improvement in spatial distribution over the existing species composition data set at a 10 × 10 km resolution from the previous Canadian forest inventory (CanFI) (Gillis et al. 2005) or its enhancement to 250 × 250 m resolution through randomized predictions (Yemshanov et al. 2011).

One of the strengths of the *k*NN approach is that it supports the identification of undersampled areas or forest types through the use of various diagnostic variables (McRoberts 2009, 2012). Our results show that the geographic recruitment distances of the k pixels increase with a decrease in the density of PP, a situation that also

Fig. 4. Maps of *k*NN prediction across the 12 forested ecozones of Canada along with three diagnostic variables for total live aboveground biomass (AGB, t/ha): (A) predicted AGB; (B) CV% according to eqs. 4*a* and 4*b*; (C) mean Euclidian distance (D_{euc}); and (D) mean geographic recruitment distance (D_{geo}) of the $k = 6$ nearest neighbour reference pixels. Names are provided only for the six well-inventoried ecozones (see Fig. 1 and Table 1). (Base maps source: Natural Resources Canada under the Open Government Licence – Canada (http://data.gc.ca/eng/open-government-licence-canada.)
(Concluded on next page.)

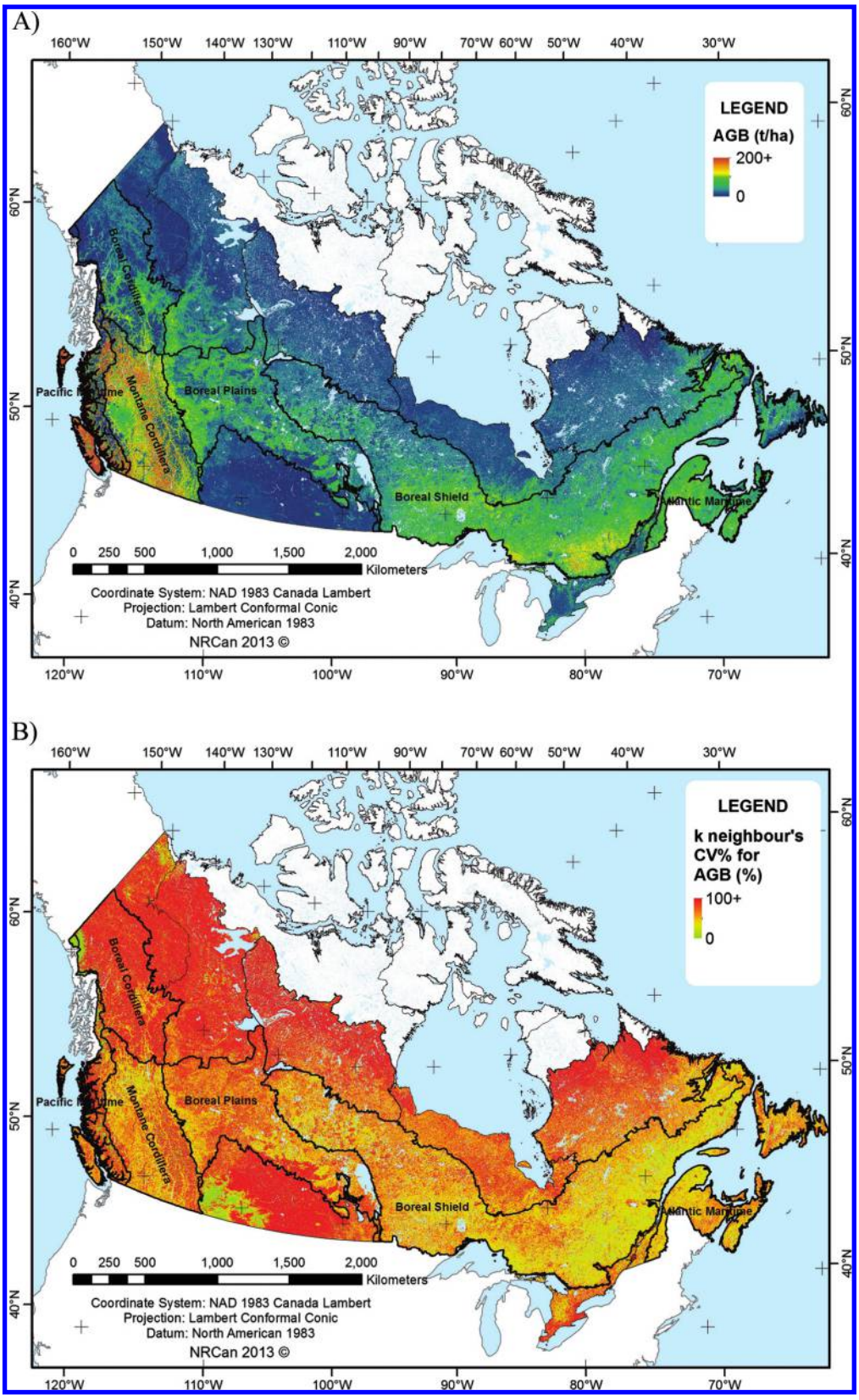

Fig. 4 (*concluded*).

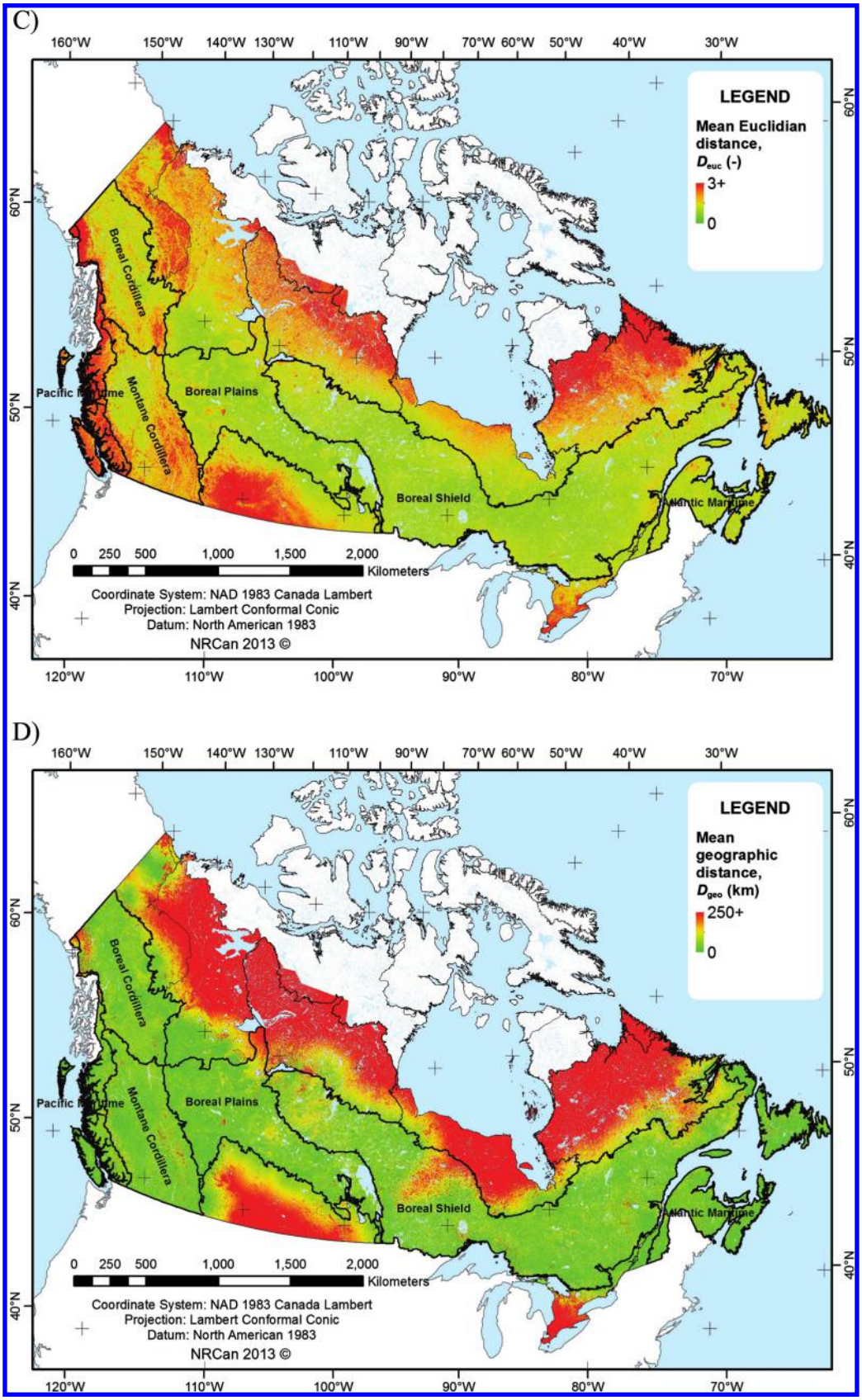

Fig. 5. Ecozone-level means of (A) three diagnostic variables based on the $k = 6$ nearest neighbour reference pixels: CV% (%, eqs. 4*a* and 4*b*), D_{euc} (–), and D_{geo} (km), and (B) three *k*NN prediction accuracy measures: $R^2 \times 100$, and RMSD% and MD%, both for six well-inventoried ecozones using the 30% validation pixels (total $N_{val} = 8508$; see Table 1 for N_{val} per ecozone). Ecozones are sorted by increasing mean observed PP aboveground biomass (AGB, t/ha) (solid circles); an asterisk (*) indicates a mountainous ecozone.

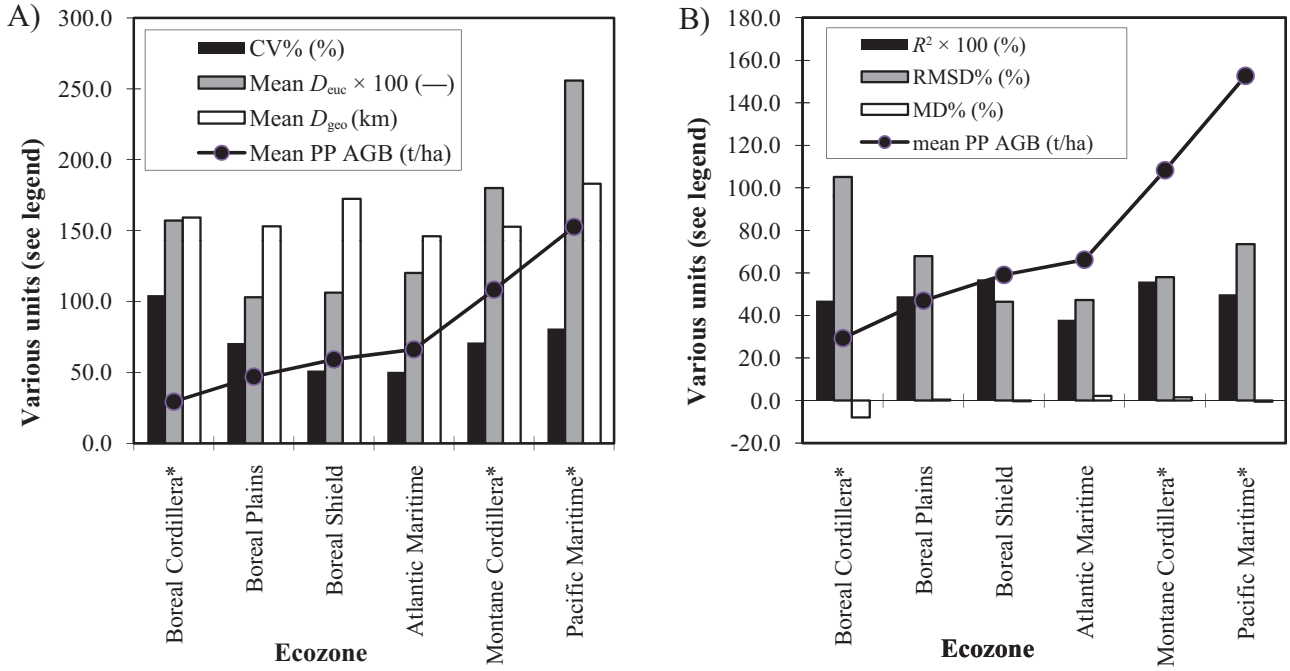

Fig. 6. Binned pixel-level observed aboveground biomass (AGB, t/ha) from PP vs. *k*NN-imputed AGB using all validation pixels (total N_{val} = 9055 of which N_{val} = 8508 for six well-inventoried ecozones). Each solid circle represents the mean of 100 binned values (±1 standard deviation). Also shown are the mean pixel-level values of R^2, MD%, and RMSD%.

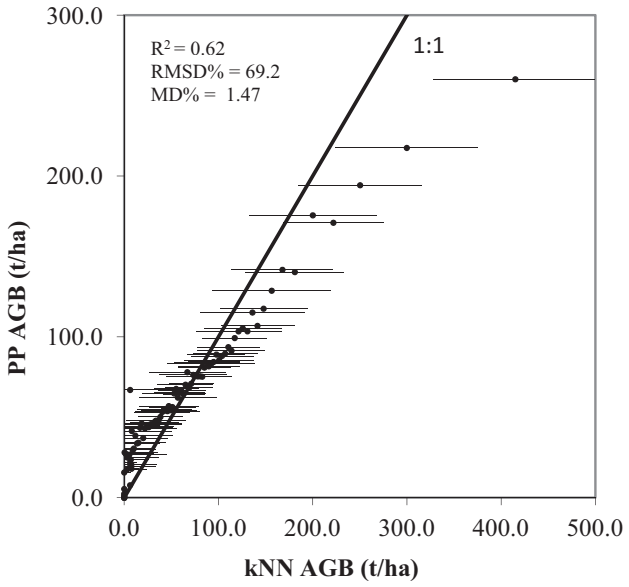

Fig. 7. Percent change in R^2, RMSD%, and MD% (absolute) for aboveground biomass (AGB) plotted against spatial resolutions obtained by aggregating pixels within 3 × 3 (750 m), 5 × 5 (1250 m), and 7 × 7 (1750 m) windows within NFI PPs ($N = 349$). Mean pixel-level values of the three accuracy measures at 250 m resolution are given in Fig. 6.

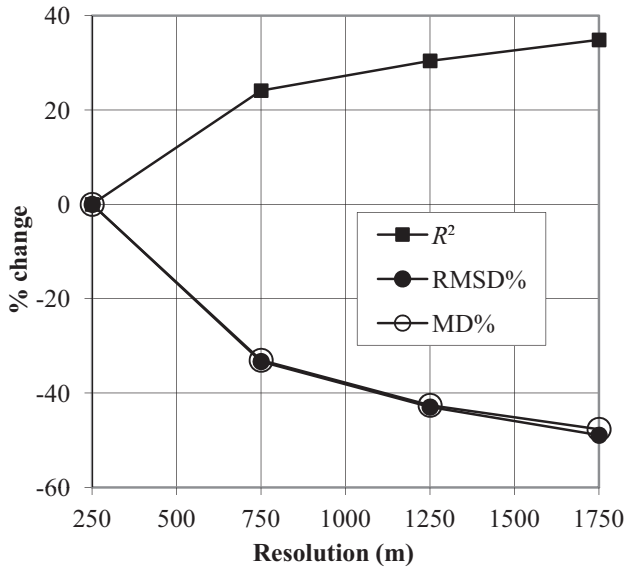

increases the probability of recruiting neighbour pixels with incorrect presence of low-abundance species. The mountainous areas of western Canada, as well as areas with low biomass, also pose a particular recruitment challenge in both the spatial and feature domains. Results indicate that the set of reference pixels in these areas is not sufficiently representative of the pixel population and is a source of significant bias (Magnussen et al. 2010).

Such information provides valuable feedback to inventory programs and can be used to target areas for further investments in monitoring, which in turn will improve *k*NN predictions.

Additional avenues for improvement include the use of radar backscatter (Holmström and Fransson 2003), forest stratification (Wilson et al. 2013), a priori information such as coarse species distribution or land cover maps (Tomppo and Halme 2004), and bias correction (Magnussen et al. 2010). Current work priorities

Table 3. Sum of total live aboveground biomass (AGB, t) for the six well-inventoried ecozones as estimated from National Forest Inventory (NFI) photo-plot (PP) values expanded to all 20 × 20 km² PP tiles for the PPs retained for *k* nearest neighbours (*k*NN) and the *k*NN pixel values summed across the same PP tiles, along with relative difference (%).

Ecozone	No. of PP tiles†	Total area of PP tiles (km²)	PP total AGB (t)	*k*NN total AGB (t)	Relative difference *k*NN–PP AGB (%)
Boreal Shield	2869	1.14×10^{6}	6.63×10^{9}	6.61×10^{9}	−0.26
Boreal Plain	1515	6.0814×10^{5}	2.65×10^{9}	2.72×10^{9}	2.38
Montane Cordillera*	1195	4.79×10^{5}	4.85×10^{9}	5.07×10^{9}	4.55
Boreal Cordillera*	1051	4.17×10^{5}	1.28×10^{9}	1.38×10^{9}	7.95
Atlantic Maritime	308	1.21×10^{5}	8.57×10^{8}	8.32×10^{8}	−2.92
Pacific Maritime*	266	1.06×10^{5}	1.30×10^{9}	1.29×10^{9}	−1.47
All	7204	2.87×10^{6}	1.78×10^{10}	1.76×10^{10}	−1.83

Note: Ecozones are sorted in decreasing number of PP tiles.

*Mountainous ecozones.

†Total number of PP tiles is lower than number of PP reported in Table 1 ($N = 7689$) as PP tiles including large water bodies (AGB = 0) were removed.

also include the generation of 2011 maps of forest attributes, as well as validation and eventually improvements of these products in the unmanaged northern ecozones (Taiga Shield, Taiga Plains, and Taiga Cordillera). The latter is an area of high priority for NFI and for carbon accounting.

In summary, the coupling of PP data with an array of feature variables through the use of the nonparametric *k*NN method can be used to produce moderate-resolution maps of forest attributes across Canada. The error structure of these products at first analysis appears close to that of regular forest inventories in Canada for key attributes. However, the continuous coverage of quantitative variables harmonized across provincial and territorial boundaries, increased timeliness through assimilation of current information at small incremental cost, and small area estimation are distinct innovations and advantages of these products in the Canadian context. As they stand, these moderate-resolution NFI map products for Canada's forest are the first of their kind and already have strategic applications in analyses that require timely spatially explicit forest information across provincial boundaries.

Acknowledgements

This project would not have been possible without the high-quality MODIS mosaics provided graciously by Darren Pouliot and Rasim Latifovic (Canada Centre for Remote Sensing of Natural Resources Canada). We also acknowledge the contribution of Dan McKenney and his team (Canadian Forest Service, Natural Resources Canada) for providing the climate-related feature variables and thank both Dan McKenney and Ron McRoberts for their reviews of this manuscript. In addition to our regular operating funds, this project was supported by the Forest Change Initiative of the Canadian Forest Service, whose confidence in this project is deeply appreciated, as well as indirectly by the National Forest Inventory (NFI) and its provincial partner agencies who provided the data foundation for this research. Finally, we express our thanks to Canadian Forest Service specialist Rémi St-Amant for the creation of the fast and efficient C++ *k*NNMapping code, without which the task of performing Canada-wide analyses would have been a significantly greater challenge.

References

Beaudoin, A., Bernier, P., Guindon, L., Villemaire, P., Hall, R.J., Arsenault, E.J., and McKenney, D. 2011. Spatialising NFI attributes across Canada through kNN imputation using MODIS, climatic and topographic geospatial layers: biomass mapping results over Quebec. *In* Proceedings of the 32nd Canadian Symposium on Remote Sensing, June 13–16, 2011, Sherbrooke, Quebec.

Bernier, P.Y., Daigle, G., Rivest, L.-P., Ung, C.-H., Labbé, F., Bergeron, C., and Patry, A. 2010. From plots to landscape: a *k*-NN-based method for estimating stand-level merchantable volume in the Province of Québec, Canada. For. Chron. **86**: 461–468.

Boudewyn, P., Song, X., Magnussen, S., and Gillis, M.D. 2007. Model-based, volume-to-biomass conversion for forested and vegetated land in Canada. Natural Resources Canada, Canadian Forest Service, Pacific Forestry Centre, Victoria, B.C., Inf. Rep. BC-X-411.

Brosofske, K.D., Froese, R.E., Falkowski, M.J., and Banskoto, A. 2014. A review of methods for mapping and prediction of inventory attributes for operational forest management. For. Sci. **60**. In press (http://www.ingentaconnect.com/content/saf/fs/pre-prints/content-forsci12134).

Crookston, N.L., and Finley, A.O. 2008. yaImpute: an R package for *k*NN imputation. J. Statistical Software, **23**: 1–16.

Dobson, M.C., Ulaby, F.T., LeToan, T., Beaudoin, A., Kasischke, E.S., and Christensen, N. 1992. Dependence of radar backscatter on coniferous forest biomass. IEEE Trans. Geosci. Remote Sensing, **30**: 412–415. doi:10.1109/36.134090.

Ecological Stratification Working Group. 1996. A national ecological framework for Canada. Agriculture and Agri-Food Canada, Research Branch, Centre for Land and Biological Resources Research and Environment Canada, State of the Environment Directorate, Ottawa, Canada.

Efron, B., Hastie, T., Johnstone, V., and Tibshirani, R. 2004. Least angle regression. Ann. Stat. **32**: 407–499. doi:10.1214/009053604000000067.

Farr, T.G., Rosen, P.A., Caro, E., Crippen, R., Duren, R., Hensley, S., Kobrick, M., Paller, M., Rodriguez, E., Roth, L., Seal, D., Shaffer, S., Shimada, J., Umland, J., Werner, M., Oskin, M., Burbank, D., and Alsdorf, D. 2007. The Shuttle Radar Topography Mission. Rev. Geophys. **45**: RG2004. doi:10.1029/2005RG000183.

Gillis, M.D., Omule, A.Y., and Brierley, T. 2005. Monitoring Canada's forests: The National Forest Inventory. For. Chron. **81**: 214–221.

Guindon, L., Pouliot, D., Beaudoin, A., Latifovic, R., Hall, R., Villemaire, P., Beaubien, J., Bernier, P., and St-Amant, R. 2011. An improved method for the annual mapping of forest disturbance across Canada based on MODIS 250 m data and decision/regression trees. *In* Proceedings of the 32nd Canadian Symposium on Remote Sensing, June 13–16, 2011, Sherbrooke, Quebec.

Hall, R.J., Skakun, R.S., Beaudoin, A., Wulder, M.A., Arsenault, E.J., Bernier, P.Y., Guindon, L., Luther, J.E., and Gillis, M.D. 2010. Approaches for forest biomass estimation and mapping in Canada. *In* Proceedings of the 30th IEEE International Geoscience and Remote Sensing Symposium, 25–30 July 2010, Honolulu, Hawaii, USA, Article No. 5650777. pp. 1988–1991. doi:10.1109/IGARSS.2010.5650777.

Holmström, H., and Fransson, J.E.S. 2003. Combining remotely sensed optical and radar data in *k*NN estimation of forest variables. For. Sci. **4**: 409–418.

Hudak, A.T., Crookston, N.L., Evans, J.S., Hall, D.E., and Falkowski, M.J. 2008. Nearest neighbour imputation of species-level, plot-scale forest structure attributes from LiDAR data. Remote Sens. Environ. **112**: 2232–2245. doi:10.1016/j.rse.2007.10.009.

Katila, M. 2006. Empirical errors of small area estimates from the multisource National Forest Inventory in Eastern Finland. Silva Fenn. **40**: 729–742.

Latifovic, R., Homer, C., Ressl, R., Pouliot, D., Hossian, S., Colditz, R., Olthof, I., Giri, C., and Victoria, A. 2012. North American Land Change Monitoring System. *In* Remote sensing of land use and land cover: principles and applications. *Edited by* C. Giri. CRC Press. pp. 303–324.

LeMay, V., and Temesgen, H. 2005. Comparison of nearest neighbor methods for estimating basal area and stems per hectare using aerial auxiliary variables. For. Sci. **51**(2): 109–119.

Lu, D., Chen, Q., Wang, G., Moran, E., Batistella, M., Zhang, M., Laurin, G.V., and Saah, D. 2012. Aboveground forest biomass estimation with Landsat and LiDAR data and uncertainty analysis of the estimates. Int. J. For. Res. **2012**: Article ID 436537. doi:10.1155/2012/436537.

Luo, Y., Trishchenko, A.P., and Khlopenkov, K.V. 2008. Developing clear-sky, cloud and cloud shadow mask for producing clear-sky composites at 250-meter spatial resolution for the seven MODIS land bands over Canada and North America. Remote Sens. Environ. **112**(12): 4167–4185. doi:10.1016/j.rse.2008.06.010.

Magnussen, S., and Russo, G. 2012. Uncertainty in photo-interpreted forest in-

ventory variables and effects on estimates of error in Canada's National Forest Inventory. For. Chron. **88**: 439–447. doi:10.5558/tfc2012-080.

Magnussen, S., Toomppo, E., and McRoberts, R.E. 2010. A model-assisted *k*-nearest neighbour approach to remove extrapolation bias. Scand. J. For. Res. **25**: 174–184. doi:10.1080/02827581003667348.

McKenney, D.W., Hutchinson, M.F., Papadopol, P., Lawrence, K., Pedlar, J., Campbell, K., Milewska, E., Hopkinson, R., Price, D., and Owen, T. 2011. Customized spatial climate models for North America. Bull. Am. Meteorol. Soc. **92**(12): 1611–1622. doi:10.1175/2011BAMS3132.1.

McRoberts, R.E. 2009. Diagnostic tools for nearest neighbors techniques when used with satellite imagery. Remote Sens. Environ. **113**: 489–499. doi:10.1016/j.rse.2008.06.015.

McRoberts, R.E. 2012. Estimating forest attribute parameters for small areas using nearest neighbors techniques. For. Ecol. Manage. **272**: 3–12. doi:10.1016/j.foreco.2011.06.039.

McRoberts, R.E., Nelson, M.D., and Wendt, D.G. 2002. Stratified estimation of forest area using satellite imagery, inventory data, and the *k*-Nearest Neighbors technique. Remote Sens. Environ. **82**: 457–468. doi:10.1016/S0034-4257(02)00064-0.

McRoberts, R.E., Tomppo, E.O., Finley, A.O., and Heikkinen, J. 2007. Estimating areal means and variances of forest attributes using the *k*-nearest neighbors technique and satellite imagery. Remote Sens. Environ. **111**: 466–480. doi:10.1016/j.rse.2007.04.002.

Mount, D.M., and Arya, S. 2010. ANN: a library for approximate nearest neighbor searching. Available from http://www.cs.umd.edu/~mount/ANN/.

National Forest Inventory. 2010. Canada's National Forest Inventory. Available at https://nfi.nfis.org.

Packanen, P., and Maltamo, M. 2007. The *k*-MSN method for the prediction of species-specific stand attributes using airborne laser scanning and aerial photographs. Remote Sens. Environ. **109**: 328–341. doi:10.1016/j.rse.2007.01.005.

Picard, R.R., and Berk, K.N. 1990. Data splitting. Am. Stat. **44**(2): 140–147. doi:10.1080/00031305.1990.10475704.

Pouliot, D., Latifovic, R., Fernandes, R., and Olthof, I. 2009. Evaluation of annual forest disturbance monitoring using a static decision tree approach and 250 m MODIS data. Remote Sens. Environ. **113**: 1749–1759. doi:10.1016/j.rse.2009.04.008.

Shimada, M., and Ohtaki, T. 2010. Generating large-scale high-quality SAR mosaic datasets: application to PALSAR data for global monitoring. IEEE J. Selected Topics in Applied Earth Observations and Remote Sensing, **3**(4): 637–656. doi:10.1109/JSTARS.2010.2077619.

Tomppo, E. 1991. Satellite image-based national forest inventory of Finland. *In* Proceedings of the Symposium on Global and Environmental Monitoring, Techniques and Impacts, 17–21 September 1990, Victoria, British Columbia, Canada. International Archives of Photogrammetry and Remote Sensing, **28**: 419–424.

Tomppo, E. 2006. The Finnish National Forest inventory. *In* Forest inventory: methodology and applications. *Edited by* A. Kangas and M. Maltamo. Springer, Dordrecht, the Netherlands.

Tomppo, E., and Halme, M. 2004. Using coarse scale forest variables as ancillary information and weighting of *k*NN estimation: a genetic algorithm approach. Remote Sens. Environ. **92**: 1–20. doi:10.1016/j.rse.2004.04.003.

Tomppo, E., Haakana, M., Katila, M., and Peräsaari, J. 2008. Multi-source national forest inventory: methods and applications. Springer.

Trishchenko, A.P., Luo, Y., and Khlopenkov, K.V. 2006. A method for downscaling MODIS land channels to 250-m spatial resolution using adaptive regression and normalization. *In* Proceedings SPIE 6366, Remote Sensing for Environmental Monitoring, GIS Applications, and Geology VI, Article No. 636607. doi:10.1117/12.689157.

Wilson, B.T., Lister, A.J., and Reimann, R.I. 2012. A nearest-neighbor imputation approach to mapping tree species over large areas using forest inventory plots and moderate resolution raster data. For. Ecol. Manage. **271**: 182–198. doi:10.1016/j.foreco.2012.02.002.

Wilson, B.T., Woodall, C.W., and Griffith, D.M. 2013. Imputing forest carbon stock estimates from inventory plots to a nationally continuous coverage. Carbon Balance Manage. **8**: 1. doi:10.1186/1750-0680-8-1.

Wulder, M.A., White, J.C., Cranny, M., Hall, R.J., Luther, J.E., Beaudoin, A., Goodenough, D.G., and Dechka, J.A. 2008. Monitoring Canada's forests. Part 1. Completion of the EOSD land cover project. Can. J. Remote Sens. **34**(6):549–562. doi:10.5589/m08-066.

Yemshanov, D., McKenney, D.W., and Pedlar, J.H. 2011. Mapping forest composition from the Canadian National Forest Inventory and land cover classification maps. Environ. Monit. Assess. **184**: 4655–4669. doi:10.1007/s10661-011-2293-2.

This article has been cited by:

1. Douglas K. Bolton, Joanne C. White, Michael A. Wulder, Nicholas C. Coops, Txomin Hermosilla, Xiaoping Yuan. 2018. Updating stand-level forest inventories using airborne laser scanning and Landsat time series data. *International Journal of Applied Earth Observation and Geoinformation* **66**, 174-183. [Crossref]
2. Qinglong Zhang, Hong S. He, Yu Liang, Todd J. Hawbaker, Paul D. Henne, Jinxun Liu, Shengli Huang, Zhiwei Wu, Chao Huang. Integrating forest inventory data and MODIS data to map species-level biomass in Chinese boreal forests. *Canadian Journal of Forest Research*, ahead of print1-19. [Abstract] [Full Text] [PDF] [PDF Plus]
3. Miren Lorente, S. Gauthier, P. Bernier, C. Ste-Marie. 2018. Tracking forest changes: Canadian Forest Service indicators of climate change. *Climatic Change* **88**. . [Crossref]
4. Junior A. Tremblay, Yan Boulanger, Dominic Cyr, Anthony R. Taylor, David T. Price, Martin-Hugues St-Laurent. 2018. Harvesting interacts with climate change to affect future habitat quality of a focal species in eastern Canada's boreal forest. *PLOS ONE* **13**:2, e0191645. [Crossref]
5. David J. Lieske, Vett K. Lloyd. 2018. Combining public participatory surveillance and occupancy modelling to predict the distributional response of Ixodes scapularis to climate change. *Ticks and Tick-borne Diseases* . [Crossref]
6. I. Aubin, L. Boisvert-Marsh, H. Kebli, D. McKenney, J. Pedlar, K. Lawrence, E. H. Hogg, Y. Boulanger, S. Gauthier, C. Ste-Marie. 2018. Tree vulnerability to climate change: improving exposure-based assessments using traits as indicators of sensitivity. *Ecosphere* **9**:2, e02108. [Crossref]
7. Kyle Lochhead, Valerie LeMay, Gary Bull, Olaf Schwab, James Halperin. Multivariate estimation for accurate and logically consistent forest-attributes maps at macroscales. *Canadian Journal of Forest Research*, ahead of print1-15. [Abstract] [Full Text] [PDF] [PDF Plus] [Supplemental Material]
8. A. Beaudoin, P.Y. Bernier, P. Villemaire, L. Guindon, X. Jing Guo. 2018. Tracking forest attributes across Canada between 2001 and 2011 using a k nearest neighbors mapping approach applied to MODIS imagery. *Canadian Journal of Forest Research* **48**:1, 85-93. [Abstract] [Full Text] [PDF] [PDF Plus] [Supplemental Material]
9. Robbie A. Hember, Nicholas C. Coops, Werner A. Kurz. 2018. Statistical performance and behaviour of environmentally-sensitive composite models of lodgepole pine growth. *Forest Ecology and Management* **408**, 157-173. [Crossref]
10. Emeline Chaste, Martin P. Girardin, Jed O. Kaplan, Jeanne Portier, Yves Bergeron, Christelle Hély. 2018. The pyrogeography of eastern boreal Canada from 1901 to 2012 simulated with the LPJ-LMfire model. *Biogeosciences* **15**:5, 1273-1292. [Crossref]
11. Daniel Fortin, Florian Barnier, Pierre Drapeau, Thierry Duchesne, Claude Dussault, Sandra Heppell, Marie-Caroline Prima, Martin-Hugues St-Laurent, Guillaume Szor. 2017. Forest productivity mitigates human disturbance effects on late-seral prey exposed to apparent competitors and predators. *Scientific Reports* **7**:1. . [Crossref]
12. Anthony R. Taylor, Yan Boulanger, David T. Price, Dominic Cyr, Elizabeth McGarrigle, Werner Rammer, John A. Kershaw. 2017. Rapid 21st century climate change projected to shift composition and growth of Canada's Acadian Forest Region. *Forest Ecology and Management* **405**, 284-294. [Crossref]
13. Yan Boulanger, Anthony R. Taylor, David T. Price, Dominic Cyr, Guillaume Sainte-Marie. 2017. Stand-level drivers most important in determining boreal forest response to climate change. *Journal of Ecology* **18**. . [Crossref]
14. Julien Beguin, Geir-Arne Fuglstad, Nicolas Mansuy, David Paré. 2017. Predicting soil properties in the Canadian boreal forest with limited data: Comparison of spatial and non-spatial statistical approaches. *Geoderma* **306**, 195-205. [Crossref]
15. Andrii Bilous, Viktor Myroniuk, Dmytrii Holiaka, Svitlana Bilous, Linda See, Dmitry Schepaschenko. 2017. Mapping growing stock volume and forest live biomass: a case study of the Polissya region of Ukraine. *Environmental Research Letters* **12**:10, 105001. [Crossref]
16. David R. Gray. 2017. Quantifying the sources of epistemic uncertainty in model predictions of insect disturbances in an uncertain climate. *Annals of Forest Science* **74**:3. . [Crossref]
17. C. B. Dean, Shelley B. Bull, Khurram Nadeem, Mark A. Wolters. Big Data in Biosciences 1-9. [Crossref]
18. J.M. Metsaranta, C.H. Shaw, W.A. Kurz, C. Boisvenue, S. Morken. 2017. Uncertainty of inventory-based estimates of the carbon dynamics of Canada's managed forest (1990–2014). *Canadian Journal of Forest Research* **47**:8, 1082-1094. [Abstract] [Full Text] [PDF] [PDF Plus] [Supplemental Material]
19. Yan Boulanger, Anthony R. Taylor, David T. Price, Dominic Cyr, Elizabeth McGarrigle, Werner Rammer, Guillaume Sainte-Marie, André Beaudoin, Luc Guindon, Nicolas Mansuy. 2017. Climate change impacts on forest landscapes along the Canadian southern boreal forest transition zone. *Landscape Ecology* **32**:7, 1415-1431. [Crossref]

20. Sander Veraverbeke, Brendan M. Rogers, Mike L. Goulden, Randi R. Jandt, Charles E. Miller, Elizabeth B. Wiggins, James T. Randerson. 2017. Lightning as a major driver of recent large fire years in North American boreal forests. *Nature Climate Change* **7**:7, 529-534. [Crossref]
21. Yan Boulanger, Martin Girardin, Pierre Y. Bernier, Sylvie Gauthier, André Beaudoin, Luc Guindon. 2017. Changes in mean forest age in Canada's forests could limit future increases in area burned but compromise potential harvestable conifer volumes. *Canadian Journal of Forest Research* **47**:6, 755-764. [Abstract] [Full Text] [PDF] [PDF Plus] [Supplemental Material]
22. A. Moreno, M. Neumann, H. Hasenauer. 2017. Forest structures across Europe. *Geoscience Data Journal* **4**:1, 17-28. [Crossref]
23. Ellen Whitman, Marc-André Parisien, David T. Price, Martin-Hugues St-Laurent, Chris J. Johnson, Evan R. DeLancey, Dominique Arseneault, Mike D. Flannigan. 2017. A framework for modeling habitat quality in disturbance-prone areas demonstrated with woodland caribou and wildfire. *Ecosphere* **8**:4, e01787. [Crossref]
24. Robbie A. Hember, Werner A. Kurz, Nicholas C. Coops. 2017. Relationships between individual-tree mortality and water-balance variables indicate positive trends in water stress-induced tree mortality across North America. *Global Change Biology* **23**:4, 1691-1710. [Crossref]
25. Pedro Rodríguez-Veiga, James Wheeler, Valentin Louis, Kevin Tansey, Heiko Balzter. 2017. Quantifying Forest Biomass Carbon Stocks From Space. *Current Forestry Reports* **3**:1, 1-18. [Crossref]
26. Susan E. Ziegler, Ronald Benner, Sharon A. Billings, Kate A. Edwards, Michael Philben, Xinbiao Zhu, Jerome Laganière. 2017. Climate Warming Can Accelerate Carbon Fluxes without Changing Soil Carbon Stocks. *Frontiers in Earth Science* **5**. . [Crossref]
27. Nicolas Mansuy, David Paré, Evelyne Thiffault, Pierre Y. Bernier, Guillaume Cyr, Francis Manka, Benoit Lafleur, Luc Guindon. 2017. Estimating the spatial distribution and locating hotspots of forest biomass from harvest residues and fire-damaged stands in Canada's managed forests. *Biomass and Bioenergy* **97**, 90-99. [Crossref]
28. Evelyne Thiffault, Kara Webster, Benoit Lafleur, Stephanie Wilson, Nicolas Mansuy. 2017. Biophysical indicators based on spatial hierarchy for informing land reclamation: The case of the Lower Athabasca River (Alberta, Canada). *Ecological Indicators* **72**, 173-184. [Crossref]
29. Juha M. Metsaranta, Carolyn E. Smyth, Werner A. Kurz. Canada 107-119. [Crossref]
30. Dinesh Babu Irulappa Pillai Vijayakumar, Frédéric Raulier, Pierre Bernier, Sylvie Gauthier, Yves Bergeron, David Pothier. 2017. Fire disturbance data improves the accuracy of remotely sensed estimates of aboveground biomass for boreal forests in eastern Canada. *Remote Sensing Applications: Society and Environment* **8**, 71. [Crossref]
31. Martin P. Girardin, Olivier Bouriaud, Edward H. Hogg, Werner Kurz, Niklaus E. Zimmermann, Juha M. Metsaranta, Rogier de Jong, David C. Frank, Jan Esper, Ulf Büntgen, Xiao Jing Guo, Jagtar Bhatti. 2016. No growth stimulation of Canada's boreal forest under half-century of combined warming and CO 2 fertilization. *Proceedings of the National Academy of Sciences* **113**:52, E8406-E8414. [Crossref]
32. Pierre Bernier, Sylvie Gauthier, Pierre-Olivier Jean, Francis Manka, Yan Boulanger, André Beaudoin, Luc Guindon. 2016. Mapping Local Effects of Forest Properties on Fire Risk across Canada. *Forests* **7**:12, 157. [Crossref]
33. Annie Bélisle, Alain Leduc, Sylvie Gauthier, Mélanie Desrochers, Nicolas Mansuy, Hubert Morin, Yves Bergeron. 2016. Detecting Local Drivers of Fire Cycle Heterogeneity in Boreal Forests: A Scale Issue. *Forests* **7**:12, 139. [Crossref]
34. Guillermo Castilla, Sebastien Rodrigue, Rob Skakun, Ron Hall. 2016. Four National Maps of Broad Forest Type Provide Inconsistent Answers to the Question of What Burns in Canada. *Remote Sensing* **8**:12, 539. [Crossref]
35. D. W. Goodsman, D. Koch, C. Whitehouse, M. L. Evenden, B. J. Cooke, M. A. Lewis. 2016. Aggregation and a strong Allee effect in a cooperative outbreak insect. *Ecological Applications* **26**:8, 2623-2636. [Crossref]
36. K. P. Bleiker, B. H. Van Hezewijk. 2016. Flight Period of Mountain Pine Beetle (Coleoptera: Curculionidae) in its Recently Expanded Range. *Environmental Entomology* **45**:6, 1561-1567. [Crossref]
37. Jeanne Portier, Sylvie Gauthier, Alain Leduc, Dominique Arseneault, Yves Bergeron. 2016. Fire Regime along Latitudinal Gradients of Continuous to Discontinuous Coniferous Boreal Forests in Eastern Canada. *Forests* **7**:12, 211. [Crossref]
38. Johann M. Housset, Christopher Carcaillet, Martin P. Girardin, Huaitong Xu, Francine Tremblay, Yves Bergeron. 2016. In situ Comparison of Tree-Ring Responses to Climate and Population Genetics: The Need to Control for Local Climate and Site Variables. *Frontiers in Ecology and Evolution* **4**. . [Crossref]
39. Anu Akujärvi, Aleksi Lehtonen, Jari Liski. 2016. Ecosystem services of boreal forests – Carbon budget mapping at high resolution. *Journal of Environmental Management* **181**, 498-514. [Crossref]
40. Jurjen van der Sluijs, Ronald J. Hall, Derek R. Peddle. 2016. Influence of Field-Based Species Composition and Understory Descriptions on Spectral Mixture Analysis of Tree Species in the Northwest Territories, Canada. *Canadian Journal of Remote Sensing* **42**:5, 591-609. [Crossref]

41. Craig Mahoney, Christopher Hopkinson, Alex Held, Marc Simard. 2016. Continental-Scale Canopy Height Modeling by Integrating National, Spaceborne, and Airborne LiDAR Data. *Canadian Journal of Remote Sensing* **42**:5, 574-590. [Crossref]
42. Dan K. Thompson, Brian N. Simpson, André Beaudoin. 2016. Using forest structure to predict the distribution of treed boreal peatlands in Canada. *Forest Ecology and Management* **372**, 19-27. [Crossref]
43. L. DOrangeville, L. Duchesne, D. Houle, D. Kneeshaw, B. Cote, N. Pederson. 2016. Northeastern North America as a potential refugium for boreal forests in a warming climate. *Science* **352**:6292, 1452-1455. [Crossref]
44. Brenda Salmón Rivera, Martin Barrette, Nelson Thiffault. 2016. Issues and perspectives on the use of exotic species in the sustainable management of Canadian forests. *Reforesta* :1, 261-280. [Crossref]
45. Olivier Blarquez, Julie C. Aleman. 2016. Tree biomass reconstruction shows no lag in postglacial afforestation of eastern Canada. *Canadian Journal of Forest Research* **46**:4, 485-498. [Abstract] [Full Text] [PDF] [PDF Plus] [Supplemental Material]
46. Shu-Jie Zhang, A-Xing Zhu, Jing Liu, Lin Yang, Cheng-Zhi Qin, Yi-Ming An. 2016. An heuristic uncertainty directed field sampling design for digital soil mapping. *Geoderma* **267**, 123-136. [Crossref]
47. Gherardo Chirici, Matteo Mura, Daniel McInerney, Nicolas Py, Erkki O. Tomppo, Lars T. Waser, Davide Travaglini, Ronald E. McRoberts. 2016. A meta-analysis and review of the literature on the k-Nearest Neighbors technique for forestry applications that use remotely sensed data. *Remote Sensing of Environment* **176**, 282-294. [Crossref]
48. Yan Boulanger, David R. Gray, Barry J. Cooke, Louis De Grandpré. 2016. Model-specification uncertainty in future forest pest outbreak. *Global Change Biology* **22**:4, 1595-1607. [Crossref]
49. Harold S.J. Zald, Michael A. Wulder, Joanne C. White, Thomas Hilker, Txomin Hermosilla, Geordie W. Hobart, Nicholas C. Coops. 2016. Integrating Landsat pixel composites and change metrics with lidar plots to predictively map forest structure and aboveground biomass in Saskatchewan, Canada. *Remote Sensing of Environment* **176**, 188-201. [Crossref]
50. Brandon Heung, Hung Chak Ho, Jin Zhang, Anders Knudby, Chuck E. Bulmer, Margaret G. Schmidt. 2016. An overview and comparison of machine-learning techniques for classification purposes in digital soil mapping. *Geoderma* **265**, 62-77. [Crossref]
51. Gherardo Chirici, Ronald E. McRoberts, Lorenzo Fattorini, Matteo Mura, Marco Marchetti. 2016. Comparing echo-based and canopy height model-based metrics for enhancing estimation of forest aboveground biomass in a model-assisted framework. *Remote Sensing of Environment* **174**, 1-9. [Crossref]
52. Martin P. Girardin, Edward H. Hogg, Pierre Y. Bernier, Werner A. Kurz, Xiao Jing Guo, Guillaume Cyr. 2016. Negative impacts of high temperatures on growth of black spruce forests intensify with the anticipated climate warming. *Global Change Biology* **22**:2, 627-643. [Crossref]
53. Graham Stinson, Steen Magnussen, Paul Boudewyn, Frank Eichel, Glenda Russo, Morgan Cranny, Alex Song. Canada 233-247. [Crossref]
54. Dinesh Babu Irulappa Pillai Vijayakumar, Frédéric Raulier, Pierre Bernier, David Paré, Sylvie Gauthier, Yves Bergeron, David Pothier. 2016. Cover density recovery after fire disturbance controls landscape aboveground biomass carbon in the boreal forest of eastern Canada. *Forest Ecology and Management* **360**, 170-180. [Crossref]
55. Dominique Guyon, Nathalie Bréda. Applications of Multispectral Optical Satellite Imaging in Forestry 249-329. [Crossref]
56. Shinya Tanaka, Tomoaki Takahashi, Tomohiro Nishizono, Fumiaki Kitahara, Hideki Saito, Toshiro Iehara, Eiji Kodani, Yoshio Awaya. 2015. Stand Volume Estimation Using the k-NN Technique Combined with Forest Inventory Data, Satellite Image Data and Additional Feature Variables. *Remote Sensing* **7**:12, 378-394. [Crossref]
57. Jean-Sébastien Landry, Navin Ramankutty. 2015. Carbon Cycling, Climate Regulation, and Disturbances in Canadian Forests: Scientific Principles for Management. *Land* **4**:4, 83-118. [Crossref]
58. Ernest William Mauya, Liviu Theodor Ene, Ole Martin Bollandsås, Terje Gobakken, Erik Næsset, Rogers Ernest Malimbwi, Eliakimu Zahabu. 2015. Modelling aboveground forest biomass using airborne laser scanner data in the miombo woodlands of Tanzania. *Carbon Balance and Management* **10**:1. . [Crossref]
59. David M. Bell, Matthew J. Gregory, Janet L. Ohmann. 2015. Imputed forest structure uncertainty varies across elevational and longitudinal gradients in the western Cascade Mountains, Oregon, USA. *Forest Ecology and Management* **358**, 154-164. [Crossref]
60. S. Gauthier, P.Y. Bernier, Y. Boulanger, J. Guo, L. Guindon, A. Beaudoin, D. Boucher. 2015. Vulnerability of timber supply to projected changes in fire regime in Canada's managed forests. *Canadian Journal of Forest Research* **45**:11, 1439-1447. [Abstract] [Full Text] [PDF] [PDF Plus] [Supplemental Material]
61. Olivier Blarquez, Adam A. Ali, Martin P. Girardin, Pierre Grondin, Bianca Fréchette, Yves Bergeron, Christelle Hély. 2015. Regional paleofire regimes affected by non-uniform climate, vegetation and human drivers. *Scientific Reports* **5**:1. . [Crossref]
62. Maurizio Santoro, André Beaudoin, Christian Beer, Oliver Cartus, Johan E.S. Fransson, Ronald J. Hall, Carsten Pathe, Christiane Schmullius, Dmitry Schepaschenko, Anatoly Shvidenko, Martin Thurner, Urs Wegmüller. 2015. Forest growing stock volume

of the northern hemisphere: Spatially explicit estimates for 2010 derived from Envisat ASAR. *Remote Sensing of Environment* **168**, 316-334. [Crossref]

63. Nicolas Mansuy, Evelyne Thiffault, Sébastien Lemieux, Francis Manka, David Paré, Luc Lebel. 2015. Sustainable biomass supply chains from salvage logging of fire-killed stands: A case study for wood pellet production in eastern Canada. *Applied Energy* **154**, 62-73. [Crossref]
64. S. Gauthier, P. Bernier, T. Kuuluvainen, A. Z. Shvidenko, D. G. Schepaschenko. 2015. Boreal forest health and global change. *Science* **349**:6250, 819-822. [Crossref]
65. Hank A. Margolis, Ross F. Nelson, Paul M. Montesano, André Beaudoin, Guoqing Sun, Hans-Erik Andersen, Michael A. Wulder. 2015. Combining satellite lidar, airborne lidar, and ground plots to estimate the amount and distribution of aboveground biomass in the boreal forest of North America. *Canadian Journal of Forest Research* **45**:7, 838-855. [Abstract] [Full Text] [PDF] [PDF Plus]
66. Johann M. Housset, Martin P. Girardin, Mathieu Baconnet, Christopher Carcaillet, Yves Bergeron. 2015. Unexpected warming-induced growth decline in Thuja occidentalis at its northern limits in North America. *Journal of Biogeography* **42**:7, 1233-1245. [Crossref]
67. Guodong Yin, Yuan Zhang, Yan Sun, Tao Wang, Zhenzhong Zeng, Shilong Piao. 2015. MODIS Based Estimation of Forest Aboveground Biomass in China. *PLOS ONE* **10**:6, e0130143. [Crossref]
68. Martin P. Girardin, Aurélie Terrier. 2015. Mitigating risks of future wildfires by management of the forest composition: an analysis of the offsetting potential through boreal Canada. *Climatic Change* **130**:4, 587-601. [Crossref]
69. Shanley D. Thompson, Trisalyn A. Nelson, Joanne C. White, Michael A. Wulder. 2015. Mapping Dominant Tree Species over Large Forested Areas Using Landsat Best-Available-Pixel Image Composites. *Canadian Journal of Remote Sensing* **41**:3, 203-218. [Crossref]
70. Rik Van Bogaert, Sylvie Gauthier, Frédéric Raulier, Jean-Pierre Saucier, Dominique Boucher, André Robitaille, Yves Bergeron. 2015. Exploring forest productivity at an early age after fire: a case study at the northern limit of commercial forests in Quebec. *Canadian Journal of Forest Research* **45**:5, 579-593. [Abstract] [Full Text] [PDF] [PDF Plus] [Supplemental Material]
71. Sylvie Gauthier, Frédéric Raulier, Hakim Ouzennou, Jean-Pierre Saucier. 2015. Strategic analysis of forest vulnerability to risk related to fire: an example from the coniferous boreal forest of Quebec. *Canadian Journal of Forest Research* **45**:5, 553-565. [Abstract] [Full Text] [PDF] [PDF Plus] [Supplemental Material]
72. Robert Jobidon, Yves Bergeron, André Robitaille, Frédéric Raulier, Sylvie Gauthier, Louis Imbeau, Jean-Pierre Saucier, Catherine Boudreault. 2015. A biophysical approach to delineate a northern limit to commercial forestry: the case of Quebec's boreal forest. *Canadian Journal of Forest Research* **45**:5, 515-528. [Abstract] [Full Text] [PDF] [PDF Plus]
73. D. Stralberg, S. M. Matsuoka, A. Hamann, E. M. Bayne, P. Sólymos, F. K. A. Schmiegelow, X. Wang, S. G. Cumming, S. J. Song. 2015. Projecting boreal bird responses to climate change: the signal exceeds the noise. *Ecological Applications* **25**:1, 52-69. [Crossref]
74. Kerry Anderson, Brian Simpson, Ronald J. Hall, Peter Englefield, Michael Gartrell, Juha M. Metsaranta. 2015. Integrating forest fuels and land cover data for improved estimation of fuel consumption and carbon emissions from boreal fires. *International Journal of Wildland Fire* **24**:5, 665. [Crossref]
75. Deepa S. Pureswaran, Louis De Grandpré, David Paré, Anthony Taylor, Martin Barrette, Hubert Morin, Jacques Régnière, Daniel D. Kneeshaw. 2014. Climate-induced changes in host tree-insect phenology may drive ecological state-shift in boreal forest. *Ecology* 141208133303004. [Crossref]
76. Guindon L., Bernier P.Y., Beaudoin A., Pouliot D., Villemaire P., Hall R.J., Latifovic R., St-Amant R.. 2014. Annual mapping of large forest disturbances across Canada's forests using 250 m MODIS imagery from 2000 to 2011. *Canadian Journal of Forest Research* **44**:12, 1545-1554. [Abstract] [Full Text] [PDF] [PDF Plus] [Supplemental Material]
77. Nicolas Mansuy, Evelyne Thiffault, David Paré, Pierre Bernier, Luc Guindon, Philippe Villemaire, Vincent Poirier, André Beaudoin. 2014. Digital mapping of soil properties in Canadian managed forests at 250m of resolution using the k-nearest neighbor method. *Geoderma* **235-236**, 59-73. [Crossref]
78. Andreas Hill, Jochen Breschan, Daniel Mandallaz. 2014. Accuracy Assessment of Timber Volume Maps Using Forest Inventory Data and LiDAR Canopy Height Models. *Forests* **5**:12, 2253-2275. [Crossref]
79. Denys Yemshanov, Daniel W. McKenney, Saul Fraleigh, Brian McConkey, Ted Huffman, Stephen Smith. 2014. Cost estimates of post harvest forest biomass supply for Canada. *Biomass and Bioenergy* **69**, 80-94. [Crossref]